

A modified discrete-vortex method algorithm with shedding criterion for aerodynamic coefficients prediction at high angle of attack

Thierry M. Faure^{a,*}, Laurent Dumas^a, Vincent Drouet^a, Olivier Montagnier^a

^a*Centre de Recherche de l'Armée de l'air, École de l'Air, F-13661 Salon-de-Provence, France*

Abstract

Low-order methods require less computing power than classical computational fluid dynamics and can be implemented on a laptop computer, which is needed for engineering tasks. Discrete vortex methods are such low order methods that can describe the unsteady separated flow around an airfoil. After a presentation of the leading edge suction parameter discrete vortex method, a modified algorithm is proposed, in order to reduce the computing cost, and compared with the previous one. Several reference unsteady airfoil motions are discussed in terms of gain in the computation time with comparisons between the previous scheme and the present one. The accuracy of the new method is demonstrated through aerodynamic coefficients. The application of the present discrete vortex method to a transient pitching motion of an airfoil is also presented, in order to understand the leading edge vortex formation, and its implication in terms of lift and drag coefficients. The method is not limited to unsteady or transient motions but can also simulate the flow around a constant angle of attack airfoil. In that case, an original method of fast summation of the vortices located far away from the airfoil, allows a linear dependence of the computation time versus the number of vortices shed, which is a great improvement over the quadratic dependence observed in the classical discrete vortex methods. The development of the aerodynamic coefficients with angle of attack, from values ranging between -10° and 90° , is obtained for a purely two-dimensional flow. In particular, the shape of the lift coefficient of the airfoil in the fully detached flow region is established. Comparisons with relevant experimental or computational fluid dynamics data are discussed in order to grasp the influence of upstream turbulence level and three-dimensional effects in the measured data in the fully detached flow region.

1. Introduction

The development of computational fluid dynamics, with approaches like discrete eddy simulation, large eddy simulation or direct numerical simulation, leads to very good accuracy in dynamic flow predictions. However, these approaches present a heavy computing cost and are inappropriate for laptop computers. That is the reason why low-order methods are very useful for engineering tasks. Discrete vortex methods are such useful tools which capture the flow physics by improving the potential theory with discrete vortex shedding [1]. They provide an intuitive understanding of wake rollup and development of detached flow regions.

The first analytical method for the estimate of lift coefficient of a constant angle of attack, attached flow airfoil, is the thin airfoil theory developed by Munk [2], Birnbaum [3] and Glauert [4]. The unsteady solution for the lift of an airfoil undergoing a step change in angle of attack was solved by Wagner [5]. Theodersen [6] developed a potential flow solution for a flat plate oscillating in pitch and plunge with a small-amplitude harmonic motion. Unsteady aerodynamic theories and their applications to flapping or aeroelasticity of an airfoil have been established by Garrick [7] and von Kármán and Sears [8]. These methods are valuable but are based on the potential theory, and their use is limited to fully attached flows. The adaptation of the thin airfoil theory to detached flows emerged in the 1970s with the advances of computer science, with relatively limited power at

*Corresponding author

Email address: thierry.faure@ecole-air.fr (Thierry M. Faure)

that time. Clements [9], Clements and Maull [10] and Kiya and Arie [11] introduced vortex shedding to model the flow behind a detached body. Kuwahara [12] and Sarpkaya [13] numerically studied the detached flow behind a flat plate using vortex method and conformal transform. The knowledge of the separation position on an airfoil allowed Katz [14] to adapt a discrete vortex method for a partially detached airfoil. The development of more powerful computers in this decade led flow simulations toward another way with the high-order resolution of Navier-Stokes equations with closure models. Nevertheless, discrete vortex methods came back in use recently as alternative low-order methods to classical high-order computational fluid dynamics (CFD), to address engineering issues with relevant accuracy. Ansari et al. [15], Wang and Eldredge [16], Xia and Mohseni [17], Hammer et al. [18] and Ramos-García et al. [19] developed discrete vortex methods to model leading edge vortices in unsteady flows. However, these methods are limited to start and stop criteria for the vortex shedding. Ramesh et al. [20][21] addressed this issue with the implementation of a leading edge suction parameter. That criterion allows a wide range of applications for any airfoil geometry, with sharp or rounded leading edges, and any arbitrary motion. Ramesh et al.[22] proved its robustness and its relative accuracy as long as a leading edge boundary layer separation occurs. The algorithm is based, for each time step, on iterative schemes to obtain the circulation of the last generated vortices through a converging time consuming process.

The present paper proposes a modified version of the algorithm of Ramesh et al. [20][21], where the circulations of the last shed vortices are obtained by a linear system in a more efficient way in terms of computing cost. The theoretical basis of the method is recalled with the new vortex shedding criterion algorithm. It is validated on reference unsteady test cases. The modified algorithm and the initial one are compared in terms of computation time. An application of the present algorithm to the development of a leading edge vortex on a flat plate at a large angle of attack is discussed and compared with a classical three-dimensional CFD. Finally, this computational scheme is applied to a static airfoil in an upstream flow. An original method of fast summation of the vortices located far away from the airfoil, based on a k -d tree search, is implemented. This far field wake model leads to a large decrease of computation time with a linear dependence versus the number of vortices shed. The new algorithm of discrete vortex method with shedding criterion is used to obtain the development of the two-dimensional aerodynamic coefficients with angle of attack, from attached to fully detached airfoil flows. A bell-like shape curve for the lift coefficient between 30° and 90° is found. The combined effect of the upstream turbulence level and airfoil aspect ratio on that region of lift coefficient are discussed.

2. Modified algorithm for the leading edge suction parameter discrete vortex method

2.1. Founding principles

The founding principles and calculation parameters of the leading edge suction parameter discrete vortex method (LDVM) are similar to the ones presented in Ramesh et al. [20] [21] and reminded in this section. An airfoil of chord c is placed in an upstream flow of magnitude U_∞ with an angle of attack $\alpha(t)$, the aerodynamic frame of reference is (X, Z) with X the direction of U_∞ and Z perpendicular to X (figure 1). The flow velocity components in this frame are U and W . The airfoil frame of reference is (x, z) with x the chordwise direction and z perpendicular to x , the velocity component normal to the airfoil is w . A plunging motion $h(t)$ of the airfoil along axis Z can be considered.

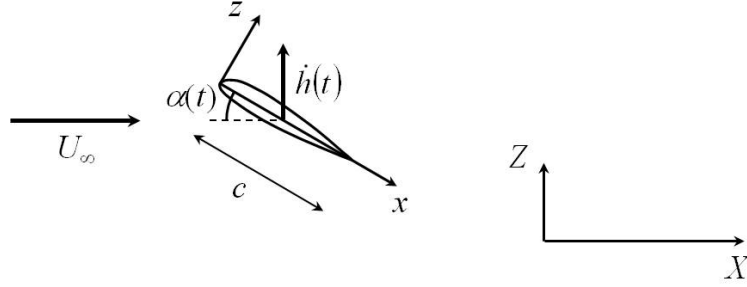
The time-dependant vorticity distribution along x is written as a Fourier series [4]:

$$\gamma(\theta, t) = 2U_\infty \left[A_0(t) \frac{1 + \cos \theta}{\sin \theta} + \sum_{n=1}^{\infty} A_n(t) \sin n\theta \right] \quad (1)$$

with the new variable θ resulting from the transformation of the chordwise coordinate x such as:

$$x = \frac{c}{2} (1 - \cos \theta)$$

The time-dependant Fourier coefficients are obtained from the velocity field $w(t)$ by enforcing the boundary condition that the flow must remain tangential to the airfoil:

Figure 1: Unsteady airfoil frame of reference (x, z) and aerodynamic frame of reference (X, Z) .

$$A_0(t) = -\frac{1}{\pi} \int_0^\pi \frac{w(\theta, t)}{U_\infty} d\theta \quad (2)$$

$$A_n(t) = \frac{2}{\pi} \int_0^\pi \frac{w(\theta, t)}{U_\infty} \cos n\theta d\theta \quad (3)$$

The induced velocity normal to the airfoil is calculated from motion kinematics [23]:

$$\begin{aligned} w(x, t) = & \frac{\partial \eta}{\partial x}(x, t) \left[\frac{\partial \Phi_{TEV}}{\partial x}(x, t) + \frac{\partial \Phi_{LEV}}{\partial x}(x, t) + U_\infty \cos \alpha(t) + \dot{h} \sin \alpha(t) \right] \\ & - \frac{\partial \Phi_{TEV}}{\partial z}(x, t) - \frac{\partial \Phi_{LEV}}{\partial z}(x, t) \\ & - U_\infty \sin \alpha(t) - \dot{\alpha}(t)(x - x_p) + \dot{h} \cos \alpha(t) \end{aligned} \quad (4)$$

where Φ_{LEV} and Φ_{TEV} are the velocity potentials associated to leading edge and trailing edge vortices, η the airfoil camberline, x_p the pivot location, $\dot{\alpha}$ the time derivative of the angle of attack corresponding to a pitch motion and \dot{h} the airfoil velocity along Z , corresponding to a plunge.

The leading edge suction parameter (LESP) is a non-dimensional measure of the suction at the leading edge [7] which is equal to the first Fourier coefficient of the vorticity distribution [21]:

$$\text{LESP}(t) = A_0(t)$$

The critical value LESP_{crit} corresponds to the A_0 value associated with the angle of attack for which spikes appear in the negative part of the friction coefficient near the leading edge suction side [21]. It is a measure of the maximum suction that a given airfoil can bear before separation and is independant of its motion [24], [25]. Parametric studies with experiments and CFD show that there is a motion independant critical value of the LESP, for a given airfoil and Reynolds number, at which leading edge vortex formation is initiated [22]. Beyond that value LESP_{crit} , the airfoil suction side boundary layer separates from the leading edge, which corresponds to the release of a leading edge vortex.

At each time step i , a trailing edge vortex (TEV) is shed. A leading edge vortex (LEV) is shed only if the LESP exceeds its critical value. The circulations associated to these LEV and TEV are obtained from Kelvin's condition:

$$\Gamma_B + \sum_{k=1}^i \Gamma_{TEV,k} + \sum_{l=1}^i \Gamma_{LEV,l} = 0 \quad (5)$$

where Γ_B is the bound circulation calculated by integrating the chordwise distribution of vorticity over the airfoil:

$$\Gamma_B = U_\infty c \pi \left[A_0(t) + \frac{A_1(t)}{2} \right] \quad (6)$$

If the LESP becomes lower than its critical value, LEV shedding is stopped. Then, the LESP concept is a single empirical parameter governing the wall viscous effect and boundary layer detachment.

In the initial LDVM of Ramesh et al. [21], the calculation of the circulation, corresponding to a vortex shed at each time step i , is obtained by a one or two-dimensional Newton-Raphson iteration, from Katz and Plotkin [23]. That iterative search, repeated at each time step, is increasing the calculation time of the flow simulation and can be avoided as presented in section 2.2.

Non-dimensional variables are introduced:

$$\begin{aligned} w^* &= \frac{w}{U_\infty} & U^* &= \frac{U}{U_\infty} & W^* &= \frac{W}{U_\infty} & X^* &= \frac{X}{c} & Z^* &= \frac{Z}{c} \\ \Gamma^* &= \frac{\Gamma}{U_\infty c} & \eta^* &= \frac{\eta}{c} & \dot{h}^* &= \frac{\dot{h}}{U_\infty} & \dot{\alpha}^* &= \frac{c}{U_\infty} \frac{d\alpha}{dt} \end{aligned}$$

The velocity induced by the k th vortex is described with the model of Vatistas et al. [26] which considers a finite core radius r_c with a solid-body rotation:

$$U_k^* = \frac{\Gamma_k^*}{2\pi} \frac{Z^* - Z_k^*}{\sqrt{[(X^* - X_k^*)^2 + (Z^* - Z_k^*)^2]^2 + r_c^{*4}}} \quad (7)$$

$$W_k^* = -\frac{\Gamma_k^*}{2\pi} \frac{X^* - X_k^*}{\sqrt{[(X^* - X_k^*)^2 + (Z^* - Z_k^*)^2]^2 + r_c^{*4}}} \quad (8)$$

with:

$$r_c^* = \frac{r_c}{c}$$

The non-dimensional time step is the same as the one used by Ramesh et al. [21]:

$$\delta t^* = \frac{\delta t U_\infty}{c} = 0.015$$

The vortex core radius is taken to be 1.3 times the average spacing between vortices, as in Leonard [27]:

$$r_c^* = \frac{r_c}{c} = 1.3 \delta t^* = 0.02$$

The location of the new k th vortex is approximated by drawing a vector from the shedding edge to the previous shed vortex and taking the position at one-third of this distance [15], for instance for the TEV:

$$\begin{aligned} X_{TEV,k}^* &= X_{TE}^* + \frac{1}{3} (X_{TEV,k-1}^* - X_{TE}^*) \\ Z_{TEV,k}^* &= Z_{TE}^* + \frac{1}{3} (Z_{TEV,k-1}^* - Z_{TE}^*) \end{aligned}$$

The advantage of the current approach is that account is taken not only of the wing motion since the last time step but also of the advection of the previous shed vortex, giving overall a more accurate depiction of the flow.

2.2. Implementation of the modified algorithm

First, consider the case with no LEV shedding ($|\text{LESP}| \leq |\text{LESP}_{crit}|$). The velocity normal to the airfoil, for time step i , is:

$$\begin{aligned}
w^*(\theta) = & \frac{\partial \eta^*}{\partial x^*}(\theta, t) \left[\cos \alpha(t) + \dot{h}^* \sin \alpha(t) + \sum_{k=1}^{i-1} U_{TEV,k}^* \cos \alpha(t) \right. \\
& - \sum_{k=1}^{i-1} W_{TEV,k}^* \sin \alpha(t) + \sum_{l=1}^{i-1} U_{LEV,l}^* \cos \alpha(t) \\
& \left. - \sum_{l=1}^{i-1} W_{LEV,l}^* \sin \alpha(t) + U_{TEV,i}^* \cos \alpha(t) - W_{TEV,i}^* \sin \alpha(t) \right] \\
& - \sin \alpha(t) - \dot{\alpha}^* [x^*(\theta) - x_p^*] + \dot{h}^* \cos \alpha(t) - \sum_{k=1}^{i-1} W_{TEV,k}^* \cos \alpha(t) \\
& - \sum_{k=1}^{i-1} U_{TEV,k}^* \sin \alpha(t) - \sum_{l=1}^{i-1} W_{LEV,l}^* \cos \alpha(t) - \sum_{l=1}^{i-1} U_{LEV,l}^* \sin \alpha(t) \\
& - W_{TEV,i}^* \cos \alpha(t) - U_{TEV,i}^* \sin \alpha(t)
\end{aligned}$$

which can be rewritten in the following form using (7) and (8):

$$w^*(\theta) = T_1 + \Gamma_{TEV,i}^* T_2 \quad (9)$$

Then, combining (2), (3), (6) and (9), the airfoil bound circulation is equal to:

$$\begin{aligned}
\Gamma_B^* &= \int_0^\pi T_1(\theta)(\cos \theta - 1) d\theta + \Gamma_{TEV,i}^* \int_0^\pi T_2(\theta)(\cos \theta - 1) d\theta \\
&= I_1 + \Gamma_{TEV,i}^* I_2
\end{aligned} \quad (10)$$

From Kelvin's theorem (5), we get:

$$\Gamma_{TEV,i}^* = -\frac{I_1 + \sum_{k=1}^{i-1} \Gamma_{TEV,k}^* + \sum_{l=1}^{i-1} \Gamma_{LEV,l}^*}{1 + I_2} \quad (11)$$

For the case where a LEV and a TEV are shed ($|\text{LESP}| > |\text{LESP}_{crit}|$), the velocity normal to the airfoil, for time step i , writes:

$$\begin{aligned}
w^*(\theta) = & \frac{\partial \eta^*}{\partial x^*}(\theta, t) \left\{ \cos \alpha(t) + \dot{h}^* \sin \alpha(t) + \sum_{k=1}^{i-1} [U_{TEV,k}^* \cos \alpha(t) \right. \\
& - W_{TEV,k}^* \sin \alpha(t)] + U_{TEV,i}^* \cos \alpha(t) - W_{TEV,i}^* \sin \alpha(t) \\
& + U_{LEV,i}^* \cos \alpha(t) - W_{LEV,i}^* \sin \alpha(t) \\
& \left. + \sum_{l=1}^{i-1} [U_{LEV,l}^* \cos \alpha(t) - W_{LEV,l}^* \sin \alpha(t)] \right\} - \sin \alpha(t) - \dot{\alpha}^* [x^*(\theta) - x_p^*] \\
& + \dot{h}^* \cos \alpha(t) - \sum_{k=1}^{i-1} [W_{TEV,k}^* \cos \alpha(t) + U_{TEV,k}^* \sin \alpha(t)] \\
& - \sum_{l=1}^{i-1} [W_{LEV,l}^* \cos \alpha(t) + U_{LEV,l}^* \sin \alpha(t)] - W_{TEV,i}^* \cos \alpha(t) \\
& - U_{TEV,i}^* \sin \alpha(t) - W_{LEV,i}^* \cos \alpha(t) - U_{LEV,i}^* \sin \alpha(t)
\end{aligned}$$

which reduces to:

$$w^*(\theta) = T_1 + \Gamma_{TEV,i}^* T_2 + \Gamma_{LEV,i}^* T_3 \quad (12)$$

The airfoil bound circulation is now:

$$\begin{aligned} \Gamma_B^* &= \int_0^\pi T_1(\theta)(\cos\theta - 1)d\theta + \Gamma_{TEV,i}^* \int_0^\pi T_2(\theta)(\cos\theta - 1)d\theta \\ &\quad + \Gamma_{LEV,i}^* \int_0^\pi T_3(\theta)(\cos\theta - 1)d\theta \\ &= I_1 + \Gamma_{TEV,i}^* I_2 + \Gamma_{LEV,i}^* I_3 \end{aligned} \quad (13)$$

The first Fourier coefficient is obtained from (2) and (12):

$$\begin{aligned} A_0(t) &= -\frac{1}{\pi} \int_0^\pi T_1(\theta)d\theta - \frac{\Gamma_{TEV,i}^*}{\pi} \int_0^\pi T_2(\theta)d\theta - \frac{\Gamma_{LEV,i}^*}{\pi} \int_0^\pi T_3(\theta)d\theta \\ &= J_1 + \Gamma_{TEV,i}^* J_2 + \Gamma_{LEV,i}^* J_3 \end{aligned} \quad (14)$$

Kelvin's theorem and the condition on the critical LESP lead to:

$$\Gamma_B^* + \Gamma_{TEV,i}^* + \Gamma_{LEV,i}^* + \sum_{l=1}^{i-1} \Gamma_{TEV,l}^* + \sum_{l=1}^{i-1} \Gamma_{LEV,l}^* = 0 \quad (15)$$

$$A_0 - \text{LESP}_{crit} = 0 \quad (16)$$

which can be written as a linear system depending only on the unknown vortex circulations for time step i :

$$I_1 + \Gamma_{TEV,i}^* (1 + I_2) + \Gamma_{LEV,i}^* (1 + I_3) + \sum_{k=1}^{i-1} \Gamma_{TEV,k}^* + \sum_{l=1}^{i-1} \Gamma_{LEV,l}^* = 0 \quad (17)$$

$$J_1 + \Gamma_{TEV,i}^* J_2 + \Gamma_{LEV,i}^* J_3 - \text{LESP}_{crit} = 0 \quad (18)$$

In addition, a condition to avoid the traversing of the camberline by a vortex has been added to the initial LDVM. Note that this change is marginal since very few vortices are following this path.

The aerodynamic normal and axial forces are obtained from the Fourier coefficients [21]:

$$\begin{aligned} F_N &= \rho U_\infty c \pi \left[(U_\infty \cos\alpha + \dot{h} \sin\alpha) \left(A_0 + \frac{A_1}{2} \right) + c \left(\frac{3\dot{A}_0}{4} + \frac{\dot{A}_1}{4} + \frac{\dot{A}_2}{8} \right) \right. \\ &\quad \left. + \rho \int_0^c \left[\left(\frac{\partial \Phi_{TEV}}{\partial x} \right) + \left(\frac{\partial \Phi_{LEV}}{\partial x} \right) \right] \gamma(x, t) dx \right] \end{aligned} \quad (19)$$

$$F_A = \rho \pi c U_\infty^2 A_0^2 \quad (20)$$

The lift and drag forces are obtained by:

$$L = F_N \cos\alpha + F_A \sin\alpha \quad (21)$$

$$D = F_N \sin\alpha - F_A \cos\alpha \quad (22)$$

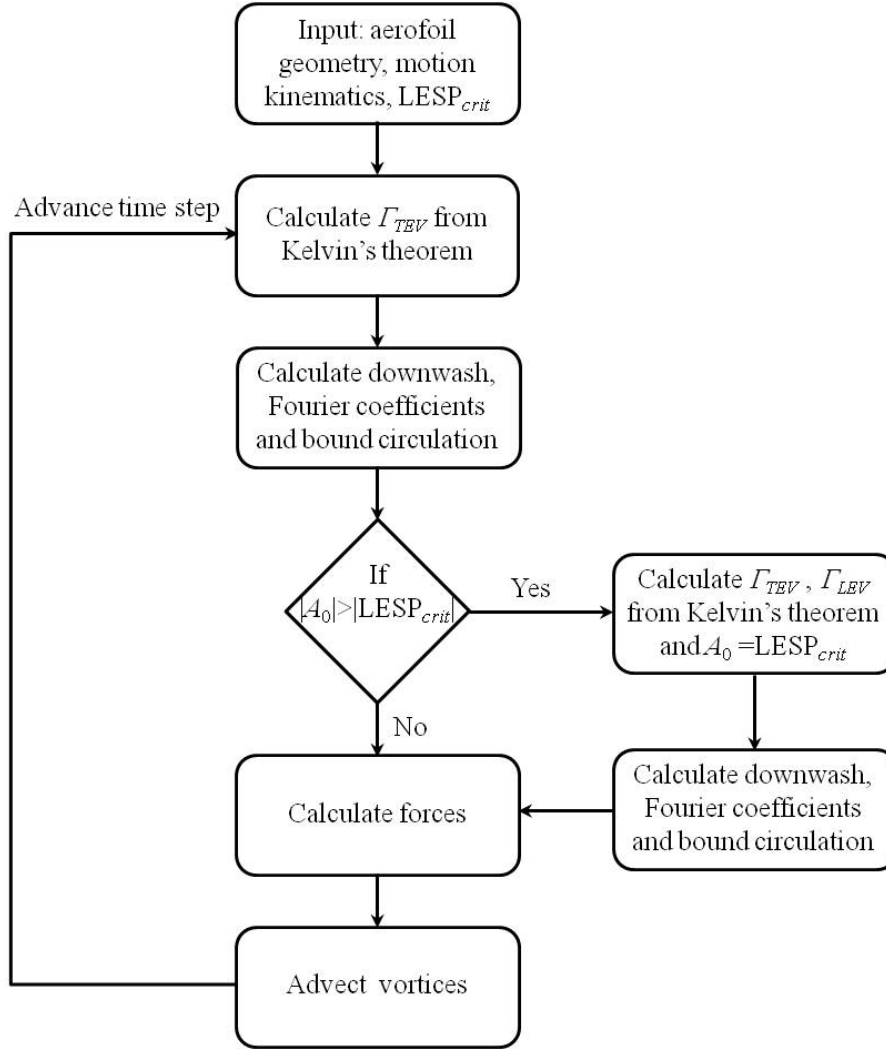


Figure 2: Flow chart of the modified LDVM algorithm.

Similarly for the pitching moment coefficient from the position x_{ref} :

$$\begin{aligned}
 M = & x_{ref} F_N - \rho \pi c^2 U_\infty \left\{ (U_\infty \cos \alpha + \dot{h} \sin \alpha) \left(\frac{A_0}{4} + \frac{A_1}{4} - \frac{A_2}{8} \right) \right. \\
 & + c \left(\frac{7A_0}{16} + \frac{3A_1}{16} + \frac{A_2}{16} - \frac{A_3}{64} \right) \\
 & \left. - \rho \int_0^c \left[\left(\frac{\partial \Phi_{TEV}}{\partial x} \right) + \left(\frac{\partial \Phi_{LEV}}{\partial x} \right) \right] \gamma(x, t) x dx \right\}
 \end{aligned} \tag{23}$$

Then, the aerodynamic coefficients C_L , C_D are obtained dividing the forces by the upstream flow dynamic pressure multiplied by the chord and the moment coefficient C_M by dividing the quarter chord moment by the upstream flow dynamic pressure multiplied by the square of the chord. The modified LDVM algorithm is presented as a flow chart in figure 2. Note that for vortex circulation computation, there is no Newton-Raphson iterative loop at each time step anymore.

3. Unsteady airfoil motions

3.1. Validation cases

The present LDVM algorithm is applied to the eight unsteady airfoil motions published in Ramesh et al. [21], to validate the accuracy of the modified algorithm. In these unsteady airfoil motions, larger values of the lift coefficients are obtained in comparison with the values obtained for a given angle of attack in steady flow. These high values can be explained by the effect of the unsteady motion and the resulting added-mass.

Case study 1 is a pitch-hold-return motion generated using the Eldredge function [28] of a SD7003 airfoil for a Reynolds number of 30000. The amplitude of the pitch is 25° with a pivot at the leading edge. The time development of angle of attack, LESP, lift, drag and quarter chord pitching moment coefficients are plotted in figure 3. Experimental data correspond to water tunnel measurements of flow visualisations by laser fluorescence and forces recordings. CFD calculations solve the time-dependant incompressible Navier-Stokes equations using a finite-volume method. All these results, with the initial LDVM are presented in Ramesh et al. [21], and are compared with the present modified LDVM algorithm.

Figure 3a shows the dimensionless time development of the angle of attack and LESP. The critical value of LESP is reached for $t^* = 2$ initiating a LEV shedding that stops at $t^* = 4.2$. Note the different angle of attack for LEV start ($\alpha = 12.9^\circ$) and stop ($\alpha = 23.9^\circ$), evidence of the unsteady effect in the lift coefficient. Similarly, the LESP is larger at the end of the run than at the beginning for the same angle of attack of 0° . The vortex shedding is initiated from the leading edge at $t^* = 2$ for $\alpha = 12.9^\circ$. It stops at $t^* = 4.2$ for $\alpha = 23.9^\circ$, but then the previously shed LEV are advected on the suction side, reflecting a partial detachment of the airfoil. Thus, a partial suction side reattachment can be considered in the method.

The lift and drag coefficients development with t^* are given in figures 3b and 3c, with comparison between experiment, CFD, LDVM of Ramesh et al. [21], and present LDVM algorithm. A very good agreement between the two LDVM algorithms is found. Both LDVM algorithms correctly capture the spikes due to apparent mass effects. Some differences with experiment and CFD in the amplitude of the coefficients are found in the downstroke for $t^* > 4$. The small discrepancies observed between present LDVM algorithm and Ramesh's LDVM lay in the iterative loops on the LEV and TEV computation present in the latter case. In particular, an exit criterion with a test on the estimated value of the circulation is necessary, leading to some discrepancies between Ramesh's algorithm and the present one, where there is no exit criterion since there is no iterative loop. Note that the discrepancies between LDVM and CFD are smaller than between CFD and experiment. Figure 3d is the non-dimensional time evolution of the quarter chord moment coefficient, for which measurements are not available. The two LDVM algorithms are very close again, and compare reasonably well with CFD except for $t^* > 4$ where C_M is more negative.

A similar agreement is found between the initial LDVM [21] and the present modified algorithm for the other seven cases, including sinusoidal pitch-plunge motions of period T , which are not presented hereafter for conciseness. We observe a relative agreement between LDVM and experiments or CFD, except for case 3C corresponding to a pitch-plunge motion of a SD7003 airfoil at a Reynolds number of 10000. In that case, the LESP never reaches its critical value, and no LEV is shed. The experiment and CFD show that a trailing edge boundary layer separation occurs. As previously observed by Ramesh et al. [21], this phenomenon is not considered in the LDVM, which explains the poor matching of the method with experiments and CFD.

The comparison of the computing times between the previous LDVM (with an iterative loop for the calculation of the circulation of each vortex shed), and the present LDVM algorithm (modified method solving a linear system for these circulations), written in the same programming language, is given in table 1. Computations are carried out, for the two algorithms, on an Intel Core i5-6300HG CPU 2.30 GHz processor with a RAM of 8 GB. The modified LDVM shows a gain in computing time generally larger than 2. This improvement on the running time of LDVM for unsteady flows, corresponding to maximum non-dimensional times of about 10, allows to extend its application to longer simulations, for transient airfoil motion. Constant angle of attack computations can be considered, in order to get spectral information such as the vortex shedding frequency of a Von K arm an vortex street.

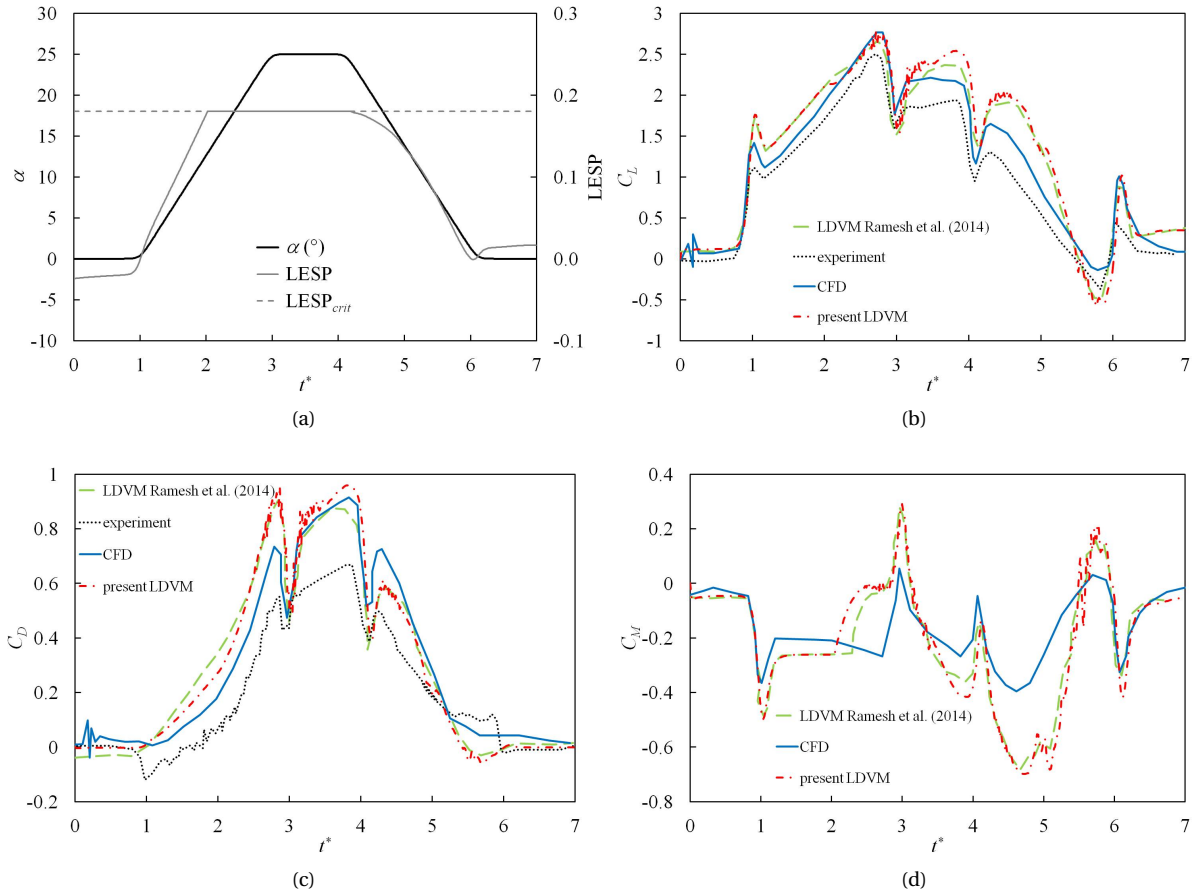


Figure 3: Case study 1 (SD7003, $Re = 30000$): time development of (a) angle of attack and LESP, (b) lift coefficient from LDVM, CFD, experiment [21] and present LDVM algorithm, (c) drag coefficient from LDVM, CFD, experiment [21] and present LDVM algorithm, (d) pitching moment coefficient about the quarter chord from LDVM, CFD [21] and present LDVM algorithm.

Case study	Airfoil	Re	$LESP_{crit}$	t_{max}^*	t/T	Time ratio
1	SD7003	30000	0.18	7	-	2.15
2	SD7003	100000	0.14	8	-	2.46
3A	SD7003	10000	0.21	-	1	1.69
3B	SD7003	10000	0.21	-	1	1.89
3C	SD7003	10000	0.21	-	1	2.08
4	NACA 0015	1100	0.19	-	1	2.41
5A	Flat plate	1000	0.11	5	-	2.69
5B	Flat plate	1000	0.11	9	-	2.70

Table 1: Comparison of the time ratios between the LDVM with an iterative loop on the vortex shedding circulation computation [21] and the present LDVM algorithm where the vortex shedding circulation computation is obtained by a linear system.

3.2. LEV formation in transient motion

The use of LDVM for longer simulation times is developed in this section, on a fast transient airfoil motion followed by a constant angle of attack position, with an application to steady flow characterization. This case corresponds to the transient pitch up motion of a flat plate of chord c with 7% thickness and sharp edges, from 0° to a given value of the angle of attack α , with a rotational speed of 120° per non-dimensional unit time, followed by a frozen position at the terminal α [29]. The center of rotation is the center of the plate. Note that the mass-added effects, corresponding to the motion of the plate, are not considered below, since the flow is discussed from $t^* = 1$, after the plate increase in angle of attack. Comparison of the two-dimensional LDVM is done with three-dimensional large eddy simulations combined with the immersed boundary technique, considering a wing of span $2c$ [29]. This simulation presents the flow field and lift and drag coefficients for Reynolds numbers equal to 440, 2000, 6000 and 21000. The present LDVM algorithm corresponds to $Re = 1000$, because the value of $LESP_{crit}$ is available only for that value of the Reynolds number in Ramesh et al. [21] (table 1), for a 2.3%-thick flat plate and with semi-circular leading and trailing edges. However, these closest conditions to CFD simulations are taken for comparison.

Figure 4 is the non-dimensional time development of the LEV for a terminal angle of attack of 25° from $t^* = 1$ to 3. Figures 4a to 4c show the vorticity obtained by three-dimensional CFD [29] at $Re = 440$ and figures 4d to 4f are the vortical centers calculated by the modified LDVM algorithm at $Re = 1000$ for the same dimensionless times. Comparing the LEV creation for Reynolds numbers between 440 and 21000, Zhang and Schlüter [29] proved that the LEV is a coherent structure undisturbed by small-scale turbulence at $Re = 440$. These authors also evidenced the influence of turbulence on the attenuation of the LEV with a positive effect on higher lift generation, and found an optimum at $Re = 2000$ where the viscosity effect is sufficiently low as not to disturb the creation of the LEV, but sufficiently large to avoid the generation of small scale turbulence. The modified LDVM presents a relatively good agreement with three-dimensional CFD. For $t^* = 1$, the LEV creation is well captured, while its chordwise extension is about $2c/3$ (figure 4d) compared to $c/2$ for CFD (figure 4a). Similarly for $t^* = 2$, the LEV covers completely the airfoil suction side (figure 4e) and only 90% in CFD (figure 4b). The slight overprediction of the LEV extension by LDVM versus CFD could be caused by a phase difference in the vortex formation and evolution, occurring at a slightly earlier time in LDVM. However, this point is not supported by the lift coefficient time development in figure 5. Another explanation for the slight overprediction of the LEV extension could be a thinner plate in LDVM than in CFD, or could be due to three-dimensional effects, not considered in that purely two-dimensional method but taken into account in CFD. For $t^* = 3$, the LEV is about to shed the wall while a TEV is forming (figure 4f). The same TEV feature is observed in CFD, with a large negative vorticity region around the trailing edge (figure 4c).

The time evolution of the lift coefficient is plotted in figure 5, exhibiting a relative agreement between the three-dimensional CFD at $Re = 440$ and present LDVM algorithm at $Re = 1000$. In particular, the same period is found, corresponding to vortex shedding. However, a periodic feature with two peaks in the amplitude of the lift coefficient is observed in CFD, evidence of the difference of the LEV and TEV influence on the airfoil, which is not identified in LDVM. This dissymmetry tends to decrease in CFD for $t^* \geq 30$.

A measure of the aerodynamic efficiency of the LEV is the maximum lift to drag ratio presented in figure 6 for different Reynolds numbers, where each point is associated with a value of the angle of attack. The maximum lift to drag ratios are obtained in the transient passing of the LEV, from its creation to its downstream shedding in the wake. The curves for $1000 \leq Re \leq 20000$ are close, including the present LDVM results. At $Re = 440$ the viscosity creates additional drag not permitting the LEV to be fully developed, resulting in lower lift to drag ratios. The relatively good fitting between three-dimensional CFD and two-dimensional LDVM could indicate that the LEV formation is essentially two-dimensional.

4. Constant angle of attack airfoil

4.1. Vortex merging

One of the main disadvantages of discrete vortex methods is the increase of computing time as the square of the number n of shedding centers, $O(n^2)$. In order to decrease this computing time for long simulations, for instance to get analysis of the shedding frequency, and keep the advantages of low-order models, it is necessary

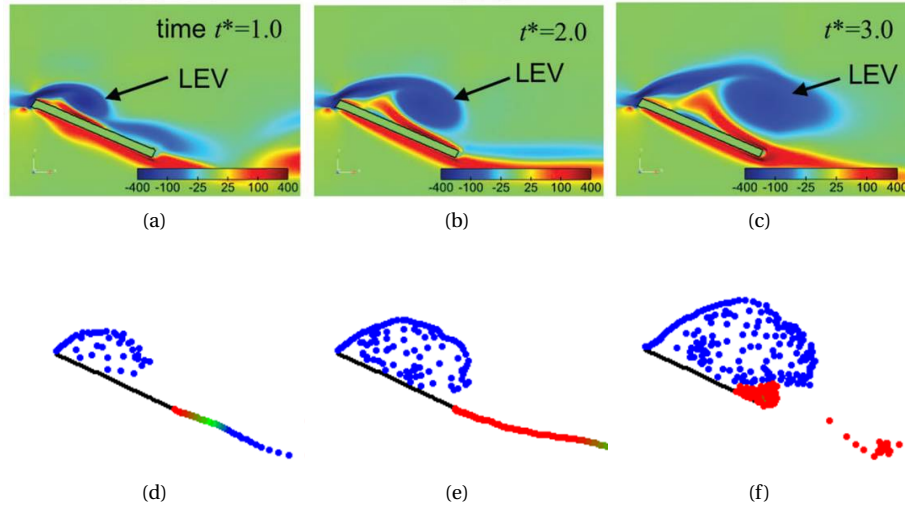


Figure 4: Vortex shedding over a flat plate pitched up to $\alpha = 25^\circ$ in a flow: spanwise vorticity contours (continuous color scale between -400 in blue and 400 in red) from CFD [29] for $Re = 440$ at (a) $t^* = 1$, (b) $t^* = 2$, (c) $t^* = 3$ and vortex circulation (negative in blue, close to 0 in green and positive in red) from present LDVM algorithm for $Re = 1000$ at (d) $t^* = 1$, (e) $t^* = 2$, (f) $t^* = 3$.

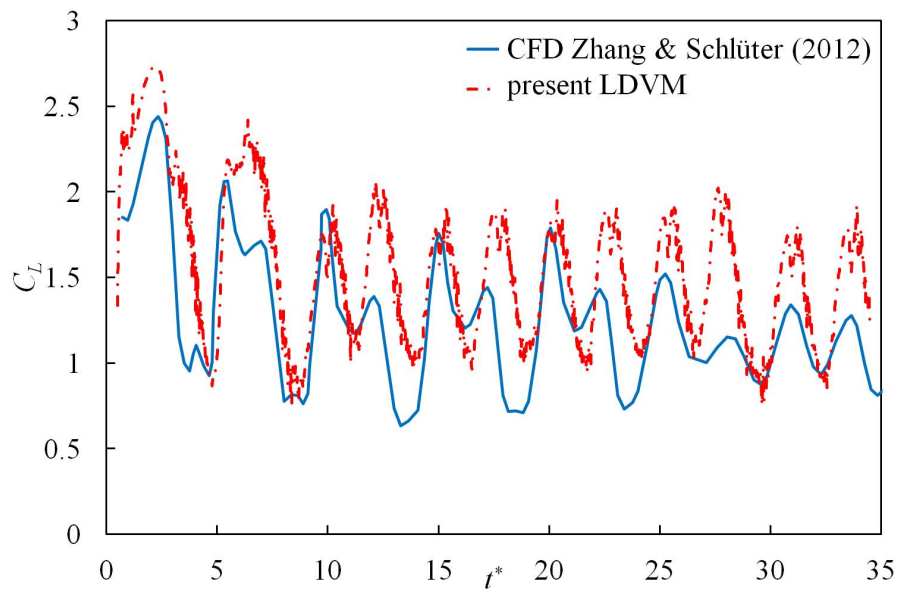


Figure 5: Comparison of the time development of the lift coefficient for a flat plate after a fast transient rotation with an angle of attack $\alpha = 25^\circ$ obtained by three-dimensional CFD at $Re = 440$ [29] and present LDVM algorithm at $Re = 1000$.

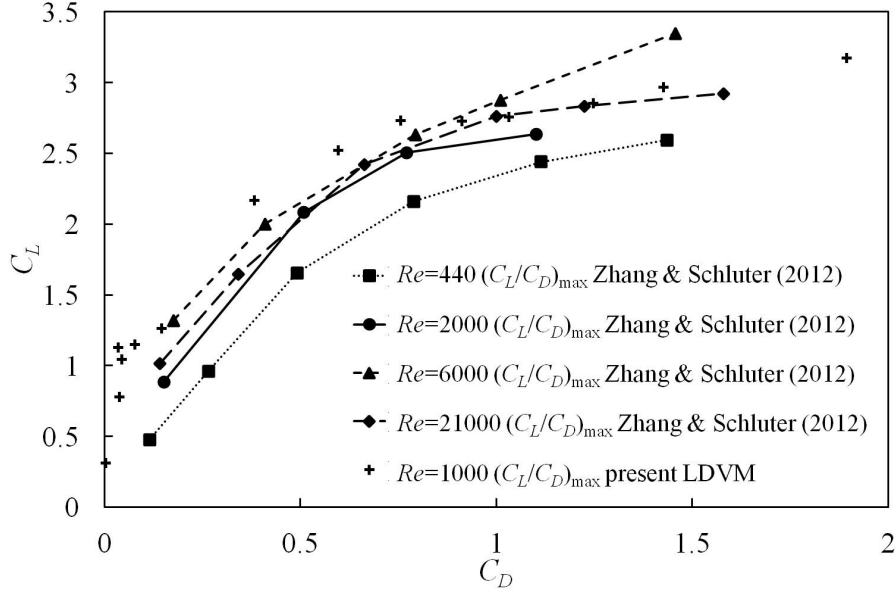


Figure 6: Maximum lift versus drag coefficient for a flat plate after a fast transient rotation at different Reynolds numbers for a three-dimensional CFD [29] compared with the present LDVM results.

to reduce the number of vortices without altering much the flow description. A deletion of the centers that exit the field of interest could be employed, but Kelvin's circulation theorem is no longer enforced for each time step, resulting in sharp peaks changes in the time development of the aerodynamic coefficients. Another option is a model reduction based on a vortex concentration. Vortex shedding from the leading edge is modeled by a shear layer that comprises few discrete vortices, concentrated in a single vortex whose strength varies with time [30]. Fast summation methods are alternative options to reduce the computation time to $O(n \log n)$ [31] or to $O(n)$ [32]. Such methods, proposed first by Sarpkaya [13], consist in a clustering of all the individual vortex centers situated downstream of a given distance downstream of the airfoil. A review of the different vortex merging methods with a discussion on their computing cost performance is available in [33]. Vortex clustering presents the advantage of not altering much the vortices near the airfoil, whose contribution is more important to aerodynamic forces, and to conserve the global circulation null. However, the way the distant vortices are removed or coalesced into an equivalent single vortex is a relevant issue. In the present study, an automatic vortex clustering method based on a k -d tree of neighboring vortices is adopted [34], which is an original application in LDVM or other potential vortex methods. For the agglomeration of vortices, several methods have been tested to travel across the tree in search for the neighbors. The most efficient method is to start with the closest vortices from the airfoil. Note that the method only takes into account the distances between vortices. Their values are used to compute the barycenter of the equivalent vortex. Once merged, the sum of the circulations of the clustered vortices is assigned to the new vortex. The relative error on aerodynamic coefficients is defined, for instance for the lift coefficient, by $\varepsilon_{C,L} = (C_{L,clust} - C_L) / C_L$, with $C_{L,clust}$ the value for vortex clustering downstream of a given distance X/c , and C_L the value without clustering. A study of the influence of the vortex merging distance showed that the relative error of the averaged aerodynamic coefficients, with and without clustering, decrease to values lower than 2% if the merging distance is $X/c > 3$ (figure 7). However, in order to keep an accurate flowfield description in the airfoil near wake, without increasing much the computing time, a merging distance $X/c = 4$ is chosen. An example is provided for a modified LDVM simulation of the flow around a SD7003 airfoil for an angle of attack of 45° at $Re = 20700$ and time $t^* = 15$ (figure 8). Without vortex merging, the airfoil suction side is completely detached and the downstream flow presents an established shedding of alternatively counter-rotating and rotating vortical structures (figure 8a). The simulation for the very same conditions but with vortex clustering beyond $X/c = 4$ is given in figure 8b. Note that the morphology of the airfoil suction side

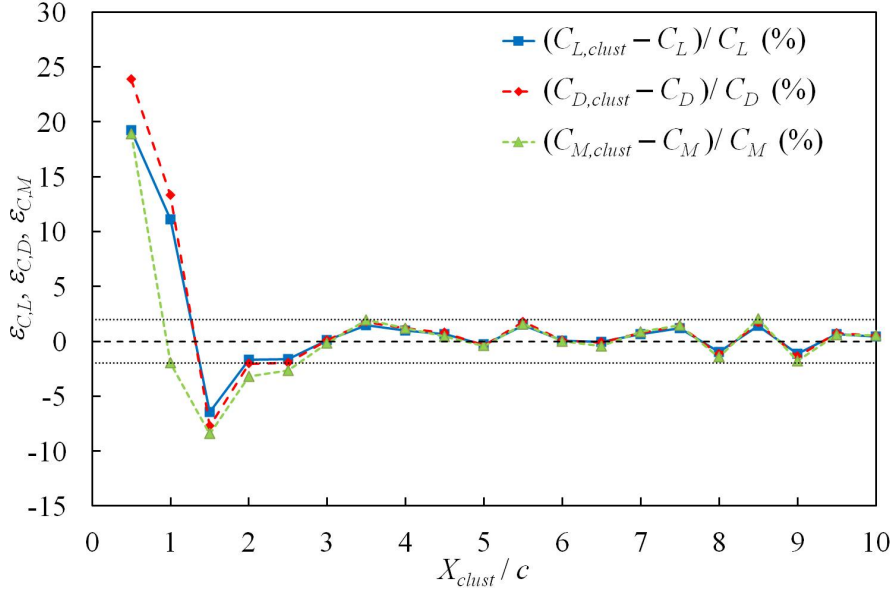


Figure 7: Relative error of the lift, drag and quarter-chord pitching moment coefficients versus clustering distance (X_{clust}/c) from the airfoil, for an angle of attack of 30° .

LEV and the last TEV and LEV produced near the airfoil is almost unchanged from the simulation without vortex merging. The LEV previously shed and located between $5 \leq X/c \leq 6$, consisting in a hundred of vortical centers, is reduced into four vortices, and similarly for the part of the TEV downstream of $X/c = 4$. Every cluster of vortices, as small as it is, is merged into at least one center. The global circulation associated with the vortical centers is conserved in the concentrated vortices. This method of vortex combination is used to save computing time and to produce a simpler picture of the vortex street.

The time development of the lift coefficient without and with vortex clustering is shown for this configuration in figure 9. The same values are obtained, with little discrepancy in some valleys where small oscillations are present. Note the physical accuracy of the vortex merging, since the same periodicity in lift coefficient variations is found with or without clustering, reflecting the large vortical structures shedding downstream of the detached flow airfoil for the large value of the angle of attack. Similar comments are valid for the drag and quarter chord moment coefficients which are not presented hereafter.

The comparison of computing times for the LDVM without and with vortex centers clustering beyond $X/c = 4$ is presented in figure 10 in linear and semi-log scales. If there is no noticeable difference in the computing time up to $t^* = 15$, there is a rapid increase for longer simulations. Without vortex merging, the computing time is increasing as the square of the number of vortices, as expected for this detached configuration with a continuous LEV and TEV shedding. With the present vortex merging method, a linear increase of the computing time with t^* is found, allowing reasonable simulation times to perform flow spectral analysis.

4.2. Aerodynamic coefficients

The lift coefficient evolution with angle of attack depends on many parameters such as airfoil shape, Reynolds number, wing aspect ratio, upstream flow turbulence level, wing surface roughness, ... Despite this, it is possible to identify three regions in this curve (figure 11), listed with increasing values of the angle of attack between 0° and 90° [35]. Region 1 is the linear part of $C_L(\alpha)$, with a slope depending on the wing aspect ratio A_R , and corresponding to attached flow conditions. Region 2 is the stall region, with a jump of lift coefficient depending on the nature of flow separation (a rapid and sharp decrease for a leading edge stall or a smoother curve for a trailing edge flow detachment). Region 3 is associated with a completely detached suction side, its bell-like

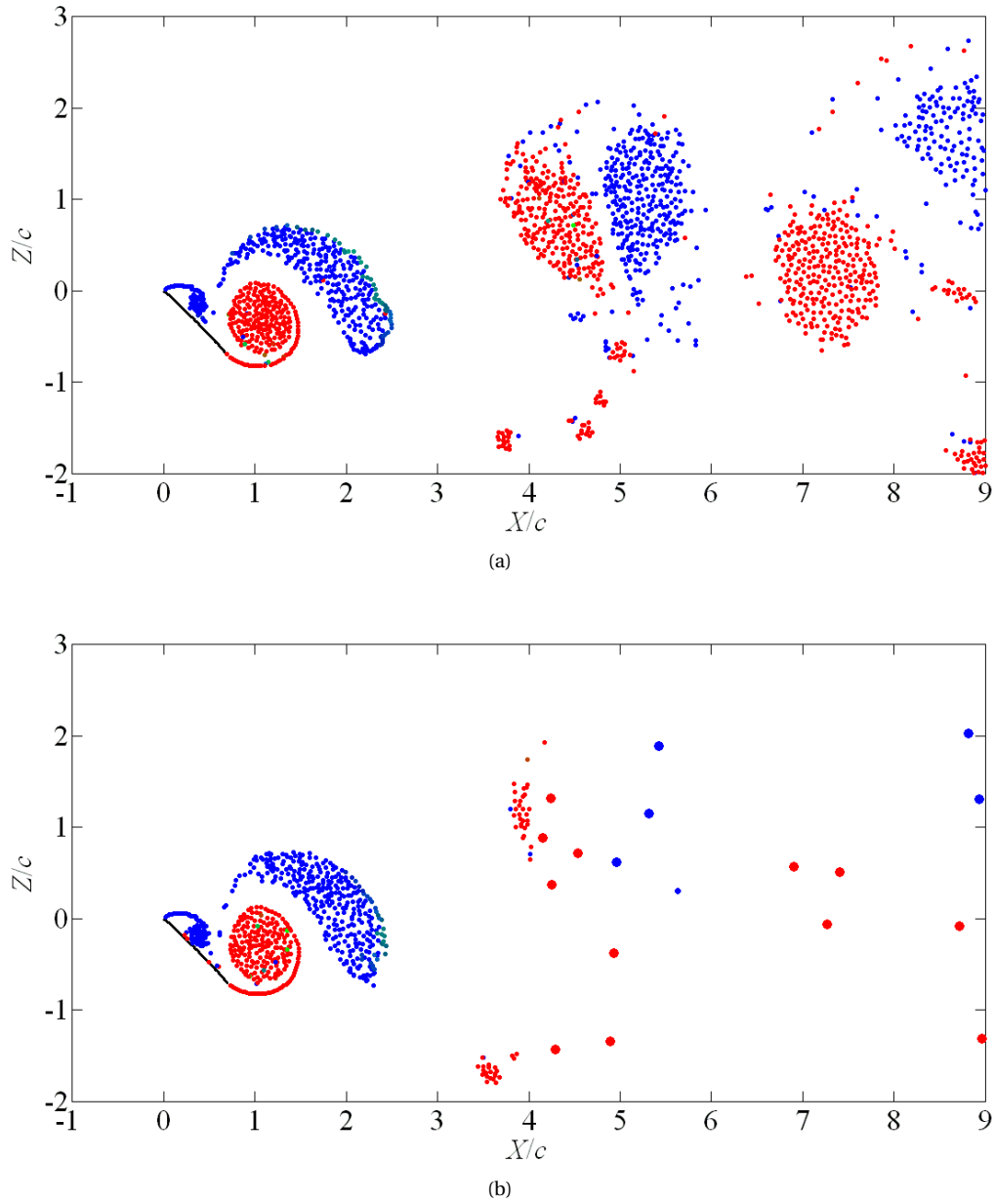


Figure 8: Flow development with vortex circulation (negative in blue, close to 0 in green and positive in red) around a SD7003 airfoil for a 45° angle of attack at $Re = 20700$ and time $t^* = 15$: (a) without vortex merging, (b) with vortex merging for $X/c > 4$.

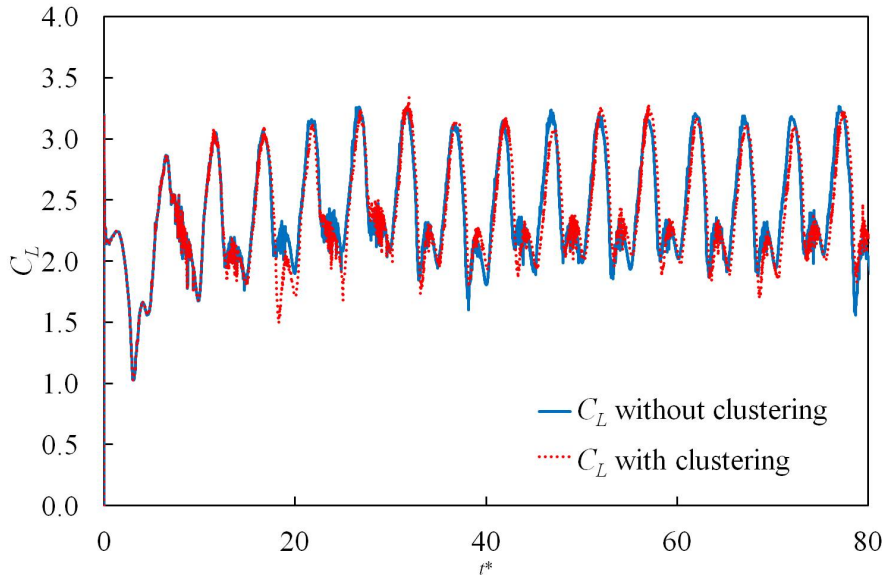


Figure 9: Time development of the lift coefficient around a SD7003 airfoil for a 45° angle of attack at $Re = 20700$ obtained from the present LDVM algorithm without and with vortex clustering downstream of $X/c = 4$.

shape is slightly dependant on the Reynolds number with a maximum lift coefficient around $\alpha \sim 40^\circ - 50^\circ$. Although different airfoils are compared, the main discrepancies concern the zero-lift angle of attack $\alpha_{L=0}$, which depends on the camber, and the stall. To get rid of the camber effect, figure 11 presents the lift coefficients plotted versus $\alpha - \alpha_{L=0}$ and we focus on the regions where the flow is attached (region 1, typically $\alpha \lesssim 15^\circ$) and fully detached (region 3, typically $\alpha \gtrsim 25^\circ$). For each value of the angle of attack, LDVM computations consider a non-dimensional simulation time $t^* = 225$ starting from rest. To eliminate the influence of the flow establishment and provide converged values, the mean coefficients are obtained by a time average between $t^* = 45$ and 225.

The measurements of Devinant et al. [35] present the lift coefficient for a thick NACA 65₄-421 airfoil with an aspect ratio of 3.67 at a Reynolds number of 2×10^5 and an upstream turbulence level of 0.5% (table 2). They are plotted for comparison with the present LDVM results for data obtained in the range 0° to 90° (figure 11). Note that in the experiment, the two-dimensional flow is obtained placing the airfoil between two parallel panels. A good agreement is found with the slope of the thin airfoil theory for the attached flow region 1 between -4° and 11° , confirming the two-dimensional flow features. However, after the stall, the flow turns three-dimensional and the accurate parameter for lift coefficient correction is the wing aspect ratio, 3.67 in this set-up, leading to relatively low lift coefficients around 1 for $\alpha = 45^\circ$. Measurements of Faure et al. [37] around a thinner NACA 23012 airfoil and a lower Reynolds number of 5.83×10^4 with an aspect ratio of 9 but without parallel end-plates show a lower slope of the curve in the attached region between 0° and 10° . After the stall drop, the lift coefficient increases and reaches a level close to the one observed in Devinant et al. [35]. For both of these experiments, region 3 corresponds to fully detached flows where two-dimensional features are no longer present. However, Laitone [36] conducted measurements around a 5% camber circular arc airfoil with a very low upstream turbulence level of 0.02%. He showed the change in the lift coefficient curves in region 3 for aspect ratios shifting from 4 to 6. Although his measurements are limited to a maximum angle of attack of 27° , the trend of convergence toward the measurements of Devinant et al. [35] for $A_R = 4$, and toward the present LDVM algorithm for $A_R = 6$, is well established. This LDVM result is also confirmed by the two-dimensional CFD of Hétru [38] around a NACA 23012 airfoil, obtained with a finite-volume Detached Eddy Simulation using CD-ADAPCO Star-CCM+. In these simulations, the two-dimensional flow feature is approached using a mesh width equal to 0.02 airfoil chord. In addition to describing well the attached flow region 1 and the stall, the simulation is converging toward LDVM

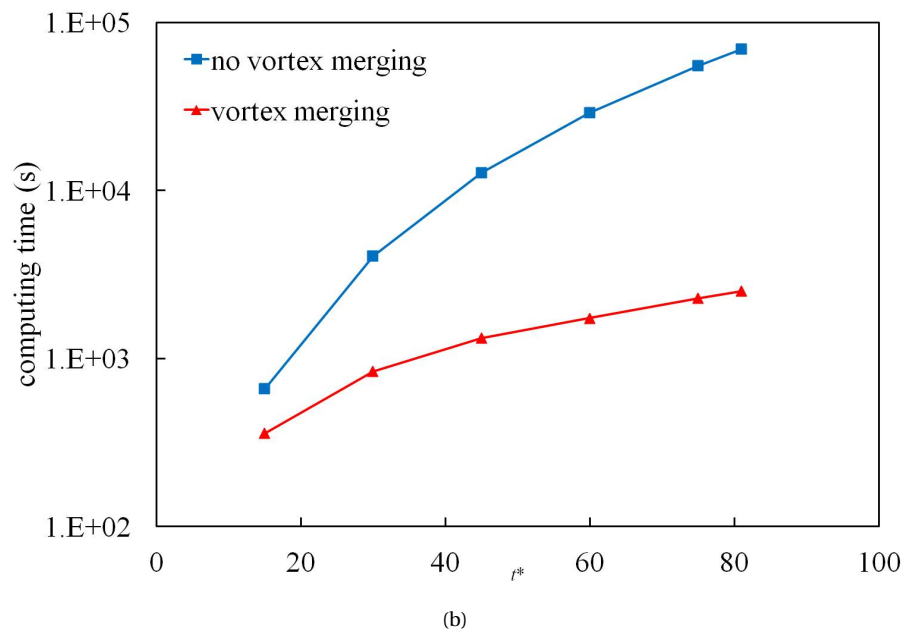
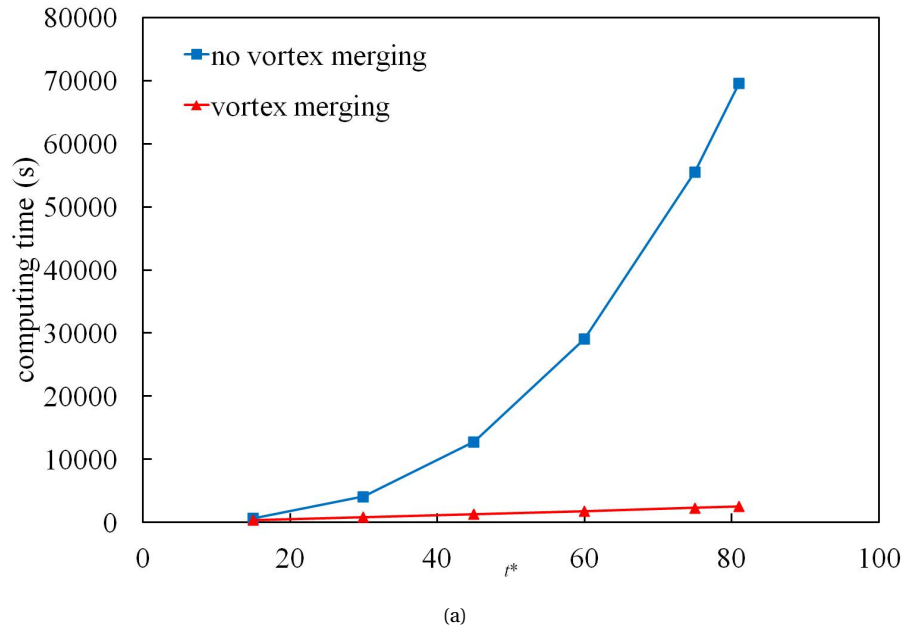


Figure 10: Computing time on a laptop configuration for the LDVM simulation of the flow around a 45° angle of attack SD7003 airfoil, with and without vortex clustering by a k -d tree search of neighboring vortices: (a) linear scale, (b) semi-log scale.

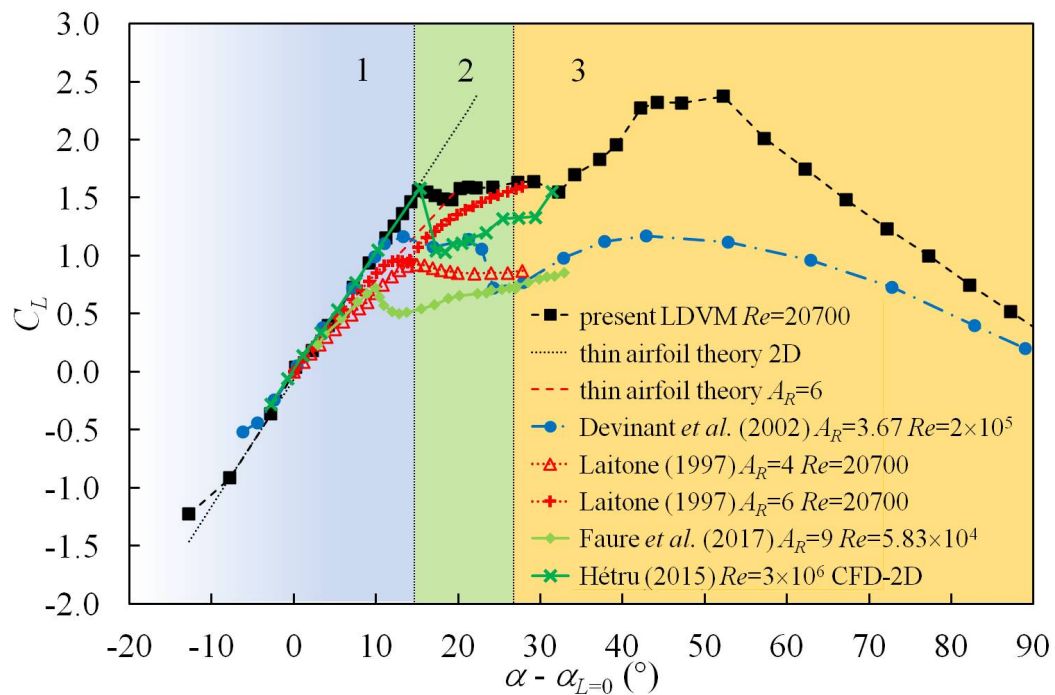


Figure 11: Lift coefficient versus corrected angle of attack $\alpha - \alpha_{L=0}$ obtained for a NACA 65_4-421 airfoil with $A_R = 3.67$ at $Re = 2 \times 10^5$ with an upstream turbulence level of 0.5% [35], for a 5% camber circular arc airfoil with $A_R = 4$ and 6 at $Re = 20700$ with an upstream turbulence level of 0.02% [36], for a NACA 23012 airfoil with $A_R = 9$ at $Re = 5.83 \times 10^4$ with an upstream turbulence level of 0.38% [37], for a two-dimensional CFD around a NACA 23012 airfoil at $Re = 3 \times 10^6$ [38], and from the present two-dimensional LDVM around a SD7003 airfoil at $Re = 20700$.

Reference	Airfoil	Re	A_R	Tu (%)	Configuration
Devinant et al. (2002) [35]	NACA 65 ₄ –421	2×10^5	3.67	0.5	Experiment
Laitone (1997) [36]	5% camber circular arc	20700	4	0.02	Experiment
Laitone (1997) [36]	5% camber circular arc	20700	6	0.02	Experiment
Faure et al. (2017) [37]	NACA 23 012	5.83×10^4	9	0.38	Experiment
Hétru (2015) [38]	NACA 23 012	3×10^6	-	-	CFD
Present study	SD 7003	20700	-	-	LDVM

Table 2: Comparison of the experimental or numerical parameters for references of figure 11: airfoil, Reynolds number, aspect ratio, up-stream flow turbulence level Tu and configuration.

results for an angle of attack of 30° . Then, the relatively large lift coefficients obtained with the present LDVM algorithm in region 3, with $C_{L,max} = 2.37$, can be related to the purely two-dimensional nature of the method.

The lift, drag and moment coefficients versus angle of attack are presented in figure 12 for a SD7003 airfoil. Measurements of Selig and Guglielmo [39] are carried out on a wing with an aspect ratio of 2.8 for a Reynolds number of 10^5 , CFD of Lian and Shyy [40] are given for similar conditions and a Reynolds number of 6×10^4 and the present LDVM results are obtained for $Re = 20700$. The accordance is perfect on lift and drag coefficients for the attached flow region. The stall angle is 13° for present LDVM algorithm and 12° for the measurements of the flow around a 5% camber of a circular arc [36] at the same Reynolds number, which justifies the comparison between these two airfoils. Measurements and CFD for a SD7003 airfoil present the stall angle of 10.5° and 11° respectively (figure 12). These discrepancies are attributed to three-dimensional effects due to a small aspect ratio of 2.8 in the experiment and CFD. Note the rapid drop in C_L for the LDVM, while measurements and CFD present a decrease in the slope of the curve $C_L(\alpha)$ before the stall point. This is typical of LDVM which considers a leading edge separation of the boundary layer without partial detachment and reattachment on the airfoil suction side. For large values of the angle of attack, the lift coefficient presents a bell-like shape with a maximum around $\alpha \sim 40^\circ - 50^\circ$ and a value close to zero for $\alpha = 90^\circ$. A good agreement is found with CFD results of Lian and Shyy [40] for the drag coefficient. This coefficient increases proportionally to the square of the angle of attack up to $\alpha = 50^\circ$ where it reaches an almost constant value. The quarter-chord pitching moment decreases from $\alpha = 15^\circ$ to 45° and gets a constant value.

5. Conclusion

A modified algorithm of the LDVM developed by Ramesh et al. [21] is proposed, leading to a smaller simulation time, reduced by a factor of about 2 for the unsteady airfoil motion test cases. The results are very similar to those obtained with the initial algorithm, and match reasonably well with available experiments or CFD as long as an initial leading edge boundary layer separation occurs. This modified LDVM is used for the study of the development of the LEV in the transient motion of a flat plate, corresponding to a pitch up motion to a frozen angle of attack. The flow features and the maximum lift versus drag coefficients, associated with a LEV formation, are in good agreement with three-dimensional CFD data obtained by Zhang and Schlütler [29]. This reflects the fact that the LEV formation is mostly two-dimensional. The present modified LDVM algorithm is also applied to constant angle of attack SD7003 airfoil flow simulations at $Re = 20700$. An original amalgamation method of the vortical centers situated sufficiently downstream of the airfoil is implemented in order to reduce the computing cost. Then, the simulation time is brought down from a dependence as the square of the number of shed vortices to a linear dependence. This reduction in computing power allows a wide range of application of the method for completely detached flows and permits spectral analysis. An important result is that the shape of the time-averaged lift coefficient after the stall, typical of aspect ratios larger than 5, is found in the present simulation. This was previously observed by Laitone [36] up to 28° but the present simulations show that the shape of the curve can be extended up to 90° . In addition, the aerodynamic coefficients fit relatively well with available

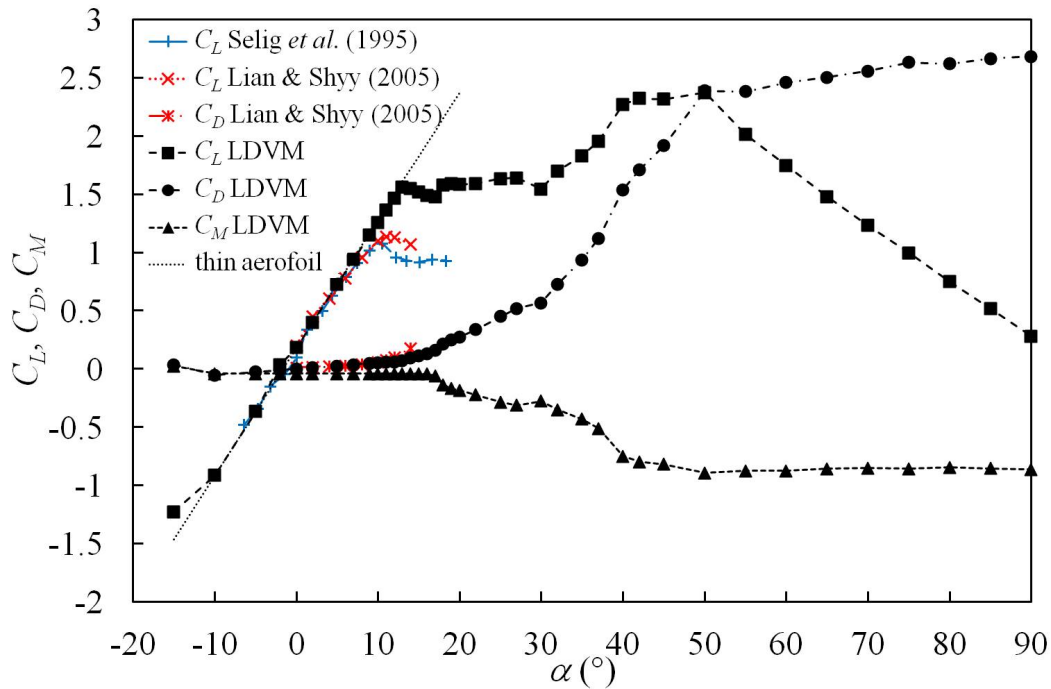


Figure 12: Lift, drag and quarter-chord moment coefficients versus angle of attack for a SD7003 airfoil obtained from experiment [39] at $Re = 10^5$, from CFD [40] at $Re = 6 \times 10^4$ and from present LDVM algorithm at $Re = 20700$.

measurements or high-order CFD for a SD7003 airfoil. The use of the LDVM is not limited to global coefficients prediction, but it is also of great interest for accurate two-dimensional flow features description. Improvements of the method, including a partial airfoil suction side detachment model, could be considered to provide a better description of the aerodynamic coefficients around the stall.

Acknowledgements

The authors wish to gratefully acknowledge the support of the Commission Armées-Jeunesse and the Bureau Armées-Nation. We thank Dr. K. Ramesh for his precisions on the method and for sharing the initial LDVM program. We thank Dr. X. Zhang and Prof. J.U. Schlüter for use of the flow plots from [29] in figure 4.

References

References

- [1] P.X. Coronado Domenge, M. Ilie, Numerical study of helicopter blade-vortex mechanism of interaction using the potential flow theory, *Appl. Math. Model.* 36 (2012) 2841–2857.
- [2] M. Munk, General theory of thin wing sections, Tech. rep., 142 NACA (1922).
- [3] W. Birnbaum, Die tragende Wirbelfläche als Hilfsmittel zur Behandlung des ebenen Problems der Tragflügeltheorie, *Z. Angew. Math. Me.* 3 (4) (1923) 290–297.
- [4] H. Glauert, The elements of aerofoil and airscrew theory, Cambridge University Press, 1926.
- [5] H. Wagner, Über die Entstehung des dynamischen Auftriebes von Tragflügeln, *Z. Angew. Math. Mech.* 5 (1) (1925) 17–35.
- [6] T. Theodorsen, General theory of aerodynamic instability and the mechanism of flutter, Tech. rep., 496 NACA (1935).
- [7] I. E. Garrick, Propulsion of a flapping and oscillating airfoil, Tech. rep., NACA TN-D-85 (1937).
- [8] T. von Kármán, W. Sears, Aerofoil theory for non-uniform motion, *J. Aero. Sci.* 5 (10) (1938) 379–390.
- [9] R. R. Clements, An inviscid model of two-dimensional vortex shedding, *J. Fluid Mech.* 57 (2) (1973) 321–336.
- [10] R. R. Clements, D. J. Maull, The representation of sheets of vorticity by discrete vortices, *Prog. Aero. Sci.* 16 (2) (1975) 129–146.

- [11] M. Kiya, M. Arie, A contribution to an inviscid vortex-shedding model for an inclined flat plate in uniform flow, *J. Fluid Mech.* 82 (2) (1977) 241–253.
- [12] K. Kuwahara, Numerical study of flow past an inclined flat plate by an inviscid model, *J. Phys. Soc. Japan* 35 (1973) 1545.
- [13] T. Sarpkaya, An inviscid model of two-dimensional vortex shedding for transient and asymptotically steady separated flow over an inclined plate, *J. Fluid Mech.* 68 (1) (1975) 109–128.
- [14] J. Katz, Discrete vortex method for the non-steady separated flow over an aerofoil, *J. Fluid Mech.* 102 (1981) 315–328.
- [15] S. A. Ansari, R. Zbikowski, K. Knowles, A nonlinear unsteady aerodynamic model for insect-like flapping wings in the hover. Part 2: implementation and validation, *Proc. Inst. Mech. Engrs.* 30 (2) (2006) 169–186.
- [16] C. Wang, J. D. Eldredge, Low-order phenomenological modelling of leading-edge vortex formation, *Theor. Comput. Fluid Dyn.* 27 (5) (2013) 577–598.
- [17] X. Xia, K. Mohseni, Lift evaluation of a two-dimensional pitching flat plate, *Phys. Fluids* 25 (2013) 091901.
- [18] P. Hammer, A. Altman, F. Eastep, Validation of a discrete vortex method for low Reynolds number unsteady flow, *AIAA J.* 52 (3) (2014) 643–649.
- [19] N. Ramos-García, H. Sarlak, S. Andersen, J. Sørensen, Simulation of the flow past a circular cylinder using an unsteady panel method, *Appl. Math. Model.* 44 (2017) 206–222.
- [20] K. Ramesh, A. Gopalarathnam, J. R. Edwards, M. V. Ol, K. Granlund, An unsteady airfoil theory applied to pitching motions validated against experiments and computation, *Theor. Comput. Fluid Dyn.* 27 (6) (2013) 843–864.
- [21] K. Ramesh, A. Gopalarathnam, K. Granlund, M. V. Ol, J. R. Edwards, Discrete-vortex method with novel shedding criterion for unsteady aerofoil flows with intermittent leading-edge vortex shedding, *J. Fluid Mech.* 751 (2014) 500–538.
- [22] K. Ramesh, K. Granlund, M. V. Ol, A. Gopalarathnam, J. R. Edwards, Leading-edge flow criticality as a governing factor in leading-edge vortex initiation in unsteady airfoil flows, *Theor. Comput. Fluid Dyn.* (2017) 1–28.
- [23] J. Katz, A. Plotkin, *Low-Speed Aerodynamics*, Cambridge University Press, 2001.
- [24] K. Ramesh, A. Gopalarathnam, M. V. Ol, K. Granlund, J. R. Edwards, Augmentation of inviscid airfoil theory to predict and model 2d unsteady vortex dominated flows, in: 41st AIAA Fluid Dynamics Conference and Exhibit, Honolulu, Hawaii, USA, 2011, AIAA Paper 2011-3578.
- [25] K. Ramesh, Theory and low-order modeling of unsteady airfoil flows, Ph.D. thesis, North Carolina State University, Raleigh, NC, USA (2013).
- [26] G. H. Vatistas, V. Kozel, W. C. Mih, A simpler model for concentrated vortices, *Exp. Fluids* 11 (1) (1991) 73–76.
- [27] A. Leonard, Vortex methods for flow simulation, *J. Comput. Phys.* 37 (3) (1980) 289–335.
- [28] J. D. Eldredge, C. J. Wang, M. V. Ol, A computational study of a canonical pitch-up, pitch down wing maneuver, 2009, AIAA Paper 2009-3687.
- [29] X. Zhang, J. Schlüter, Numerical study of the influence of the Reynolds-number on the lift created by a leading edge vortex, *Phys. Fluids* 24 (6) (2012) 065102.
- [30] A. V. SureshBabu, K. Ramesh, A. Gopalarathnam, Model reduction in discrete-vortex methods for 2D unsteady aerodynamic flows, in: 34th AIAA Applied Aerodynamics Conference, 2016, AIAA Paper 2016-4163.
- [31] J. Barnes, P. Hut, A hierarchical $O(N \log N)$ force-calculation algorithm, *Nature* 324 (1986) 446–449.
- [32] J. Carrier, L. Greengard, V. Rokhlin, A fast adaptative multipole algorithm for particle simulations, *SIAM J. Sci. and Stat. Comput.* 9 (4) (1988) 5628–5649.
- [33] P. R. Spalart, Vortex methods for separated flows, Tech. rep., Von Karman Lecture Series 1988-05 (1988).
- [34] J. L. Bentley, Multidimensional binary search trees used for associative searching, *Communications of the ACM* 18 (9) (1975) 509–517.
- [35] P. Devinant, T. Laverne, J. Hureau, Experimental study of wind-turbine airfoil aerodynamics in high turbulence, *J. Wind Eng. Ind. Aerod.* 90 (6) (2002) 689–707.
- [36] E. V. Laitone, Wind tunnel tests of wings at Reynolds numbers below 70 000, *Exp. Fluids* 23 (5) (1997) 405–409.
- [37] T. M. Faure, L. Hétru, O. Montagnier, Aerodynamic features of a two-airfoil arrangement, *Exp. Fluids* 58 (10) (2017) 146.
- [38] L. Hétru, Étude expérimentale et numérique de l'interaction aérodynamique entre deux profils : application au risque aéronautique du décrochage profond, Ph.D. thesis, Université d'Aix-Marseille, France (2015).
- [39] M. S. Selig, J. J. Guglielmo, High-lift low Reynolds number airfoil design, *J. Aircr.* 34 (1) (1997) 72–79.
- [40] Y. Lian, W. Shyy, Laminar-turbulent transition of a low Reynolds number rigid or flexible airfoil, *AIAA J.* 45 (7) (2006) 1501–1513.